Influence of projectile structure and target deformation on incomplete fusion in the $^{16}O + ^{51}V$ system

Munish Kumar,* Avinash Agarwal,† and S. Prajapati
Department of Physics, Bareilly College, Bareilly, Uttar Pradesh 243 005, India

Kamal Kumar
Department of Physics, Hindu College, Moradabad, Uttar Pradesh 244 001, India

Sunil Dutt and I. A. Rizvi
Department of Physics, Aligarh Muslim University, Aligarh, Uttar Pradesh 202 002, India

R. Kumar
NP-Group, Inter University Accelerator Center, New Delhi 110 067, India

A. K. Chaubey
Department of Physics, Addis Ababa University, P.O. Box 1176, Addis Ababa, Ethiopia

(Received 17 March 2019; published 19 September 2019)

To accomplish a systematic study of incomplete fusion, verification of more experimental data of different projectile-target combinations is required. For this purpose, the excitation functions for several evaporation residues formed in $^{16}O + ^{51}V$ interaction at energy ≈4–7 MeV/A were measured. The experimentally measured excitation functions were compared with the theoretical predictions obtained from statistical model code ALICE-91. The measured excitation functions for xn and/or pxn channels are found to be in good agreement with theoretical predictions. However, a significant enhancement has been observed for α-breakup fusion modes. This enhancement in the cross section gives clear indication of incomplete fusion of the projectile with the target. To gain insightin to the reaction dynamics, incomplete fusion probability has been deduced. This shows that the incomplete fusion process gradually increases in importance with increasing incident energy. The present results have also been compared with the results obtained in the interaction of ^{12}C and ^{20}Ne with ^{51}V where a strong projectile structure effect has been observed, which can be explained in terms of the α-decay Q value of the projectile. It is also observed that the probability of breakup of a projectile prior to fusion depends on mass asymmetry of the interacting partners as well as on the deformation of the target nucleus.

DOI: 10.1103/PhysRevC.100.034616

I. INTRODUCTION

The existence of incomplete fusion (ICF) at energies slightly above the Coulomb barrier [1–6] has led to resurgent interest in understanding the dynamics of ICF reactions in heavy-ion (HI) collisions at projectile energies varying from near to well above the Coulomb barrier. At these energies complete fusion (CF) was expected to be a dominant process; however, recent studies [7–11] show a significant contribution of ICF to the total fusion cross section (σ_{TF}). In ICF reactions, the projectile partially fuses with the target nucleusm forming an excited composite system with relatively lower mass, charge, and excitation energy compared to the completely fused composite system. Hence, the study of ICF reaction dynamics has focused attention on near-barrier energies. Britt and Quinton [12] and Galin *et al.* [13] initially observed such reactions.

Several dynamical models have been proposed from time to time to explain the ICF reaction dynamics in HI collisions, like the hot spot model [14], the sum rule model [15], the breakup fusion (BUF) model [16], the promptly emitted particles model [17] and the exciton model [18]. Out of these, the BUF and sum rule models are mostly used to study the ICF reactions dynamics, and all these models are able to fit the experimental data at energies above 10 MeV/A. In fact, there is no model available that can exactly explore the ICF reactions dynamics at near-barrier energies. Parker *et al.* [19] observed the existence of ICF in the interaction of ^{12}C, ^{15}N, ^{16}O, ^{19}F, and ^{20}Ne with a ^{51}V target at energies of 6 MeV/A. Moreover, several other studies [4–10,20–27] also found the occurrence of ICF at energies just above the Coulomb barrier. Morgenstern *et al.* [28] correlated the ICF fraction with entrance-channel mass asymmetry. Later, Singh *et al.* [29] found that the mass-asymmetry systematic may be projectile-structure dependent. Furthermore, earlier studies [20–24] also show the impact of the α-decay Q value of the projectile on ICF reaction dynamics.

*munish85physics@gmail.com
†avibcb@gmail.com

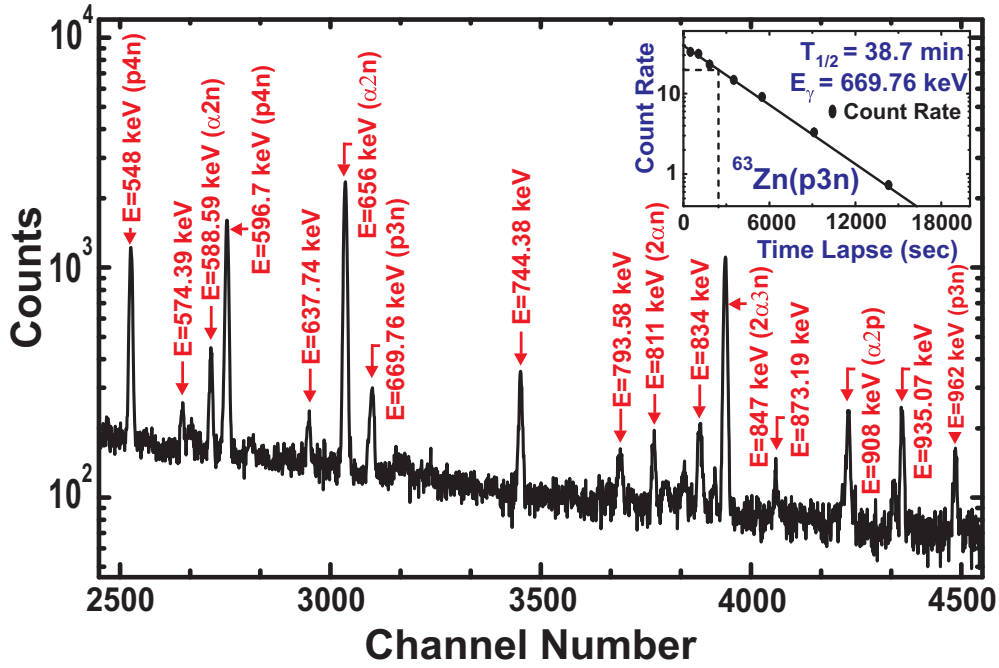

FIG. 1. Typical γ-ray spectrum of the $^{16}\mathrm{O} + {}^{51}\mathrm{V}$ system obtained at incident energy ≈100 MeV/A. The decay curve of $^{63}\mathrm{Zn}(p3n)$ residue is also shown in the inset.

The motivation of this study is to understand the ICF reactions dynamics and its dependence on various entrance channel parameters in the lower mass target region. In this regard, we have measured the excitation functions (EFs) of various evaporation residues (ERs) populated in the interaction of $^{16}\mathrm{O} + {}^{51}\mathrm{V}$. The measured EFs are then compared with the theoretical predictions obtained by employing the statistical model code ALICE-91 [30–32]. The deduced probability of ICF [$F_{\mathrm{ICF}}(\%)$] is then used for the comparative study with the available literature in terms of different entrance channel parameters. Moreover, the present work not only supplements the data of earlier work [25], but also provides a reanalyzed cross section database and presents the influence of the ICF reaction mechanism in a more conclusive way. Besides examining the effect of projectile structure on ICF reaction dynamics, an attempt has been made to explore the dependence of target deformation. The present work indicates that the mass-asymmetry systematic is affected by the target nucleus deformation parameter (β_2).

II. EXPERIMENTAL DETAILS AND DATA REDUCTION PROCEDURE

The experiment was carried out using the 15UD Pelletron accelerator at the Inter-University Accelerator Center (IUAC), New Delhi (India). Self-supporting targets of $^{51}\mathrm{V}$, each of thickness 1.987 mg/cm^2, and aluminum catcher foils, each of thickness 1.84 mg/cm^2, were prepared by the rolling technique. A stack assembly containing five target-catcher foils was irradiated by a $^{16}\mathrm{O}^{7+}$ beam at an energy ≈100 MeV for 6.35 h in the General Purpose Scattering Chamber (GPSC), which has an in-vacuum transfer facility. The main advantage of this facility is to minimize the time lapse between the stopping of irradiation and the beginning of counting. So this technique helps in counting the short-lived residues. The thickness of target and catcher foils was confirmed by the α-transmission method and chosen in such a way that it covers the desired energy range of about 4–7 MeV/A. The beam current was ≈33 nA as measured by a Faraday cup installed behind the target-catcher foil assembly. The activities produced in the individual target-catcher foil assembly were measured by using a precalibrated high-purity germanium (HPGe) detector coupled with the computer automated measurement and control (CAMAC) based data acquisition system FREEDOM developed by the IUAC [33]. The calibration of the HPGe detector was done by using a $^{152}\mathrm{Eu}$ source of known strength. The incident beam energy on each target and catcher foil was estimated by using the SRIM code [34]. The analysis of γ-ray spectra was done by using the CAMAC based data acquisition system CANDLE [35]. A typical γ-ray spectrum of $^{51}\mathrm{V}$ irradiated by the $^{16}\mathrm{O}^{7+}$ beam at energy ≈100 MeV is depicted in Fig. 1. Since it is well established that the evaporation residues populated via different reaction process decay through emission of their characteristics γ rays, the detection of γ rays gives a way to identify the populated residues by using decay curve analysis, as shown in the inset of Fig. 1. The observed intensity of activities induced in the catcher-foil assembly gives an indication of production of evaporation residues. Nuclear data like γ-ray energies, half-lives of evaporation residues, branching ratio of the γ rays, etc., used in the evaluation of experimental cross-section of identified residues populated in the present system, are taken from the *Table of Radioactive Isotopes* [36] and are listed in Table I. The standard formulation, as adopted in Refs. [5,8], was used to determine the production cross sections of various reaction products. The various factors [5] that may introduce

TABLE I. List of reaction residues with their spectroscopic properties.

ERs	Spin	Half-life	E_γ (keV)	I_γ (%)
^{65}Ga	$3/2^-$	15.2 min	115.15[a]	55.0
			153.07	9.0
			207.01	2.58
^{63}Zn	$3/2^-$	38.7 min	669.76[a]	8.4
			962.17	6.6
^{62}Zn	0^+	9.186 h	243.48	2.49
			247.01	1.88
			260.54	1.34
			394.05	2.21
			548.38	15.2
			596.70[a]	25.7
^{61}Cu	$3/2^-$	3.3 h	67.41	3.94
			282.95[a]	12.5
			373.05	2.15
			588.59	1.20
			656.01	10.66
			908.62	1.21
			1185.24	3.69
^{60}Cu	2^+	23.7 min	467.21	3.52
			497.05	1.67
			826.04	21.9
			1035.60	3.70
			1332.9[a]	88.0
^{61}Co	$7/2^-$	1.65 h	908.6[a]	3.70
^{58}Co	2^+	70.2 d	810.79[a]	99.4
^{57}Co	$7/2^-$	271.79 d	122.06[a]	85.5
			136.47	10.69
^{56}Co	4^+	77.7 d	846.81	99.9
			1037.87	14.1
			1175.15	2.26
			1238.3[a]	67.0

[a]γ lines used for data analysis.

errors and uncertainties in the cross-section measurements are the following: (i) The nonuniform thickness of samples may lead to uncertainty in determining the number of target nuclei. (ii) Fluctuation in the beam current may result in variation of the incident flux; proper care was taken to keep the beam current constant as much as possible. (iii) The dead time in the spectrometer may lead to a loss in the counts. By suitably adjusting the sample-detector distance, the dead time was kept below $\leqslant$10%. (iv) Uncertainty in determining the geometry-dependent detector efficiency may also introduce some error. (v) Errors may be due to a decrease in the oxygen ion beam intensity caused by scattering while transferring through the stack. These errors exclude uncertainty of the nuclear data, such as branching ratio, decay constant, etc., which were taken from Ref. [36]. Attempts were made to minimize the uncertainties caused by all the above factors. The overall error in the present work is estimated to be $\leqslant$17%. The measured cross section of the evaporation residues populated via CF and/or ICF processes and their comparison with the theoretical predictions may provide information about the reaction mechanism involved in the formation of residues.

III. ANALYSIS OF RESULTS WITH ALICE-91 AND THEIR INTERPRETATION

The excitation functions (EFs) of ^{65}Ga($2n$), ^{63}Zn($p3n$), ^{62}Zn($p4n$), ^{61}Cu($\alpha 2n$), ^{60}Cu($\alpha 3n$), ^{61}Co($\alpha 2p$), ^{58}Co($2\alpha n$), ^{57}Co($2\alpha 2n$), and ^{56}Co($2\alpha 3n$) evaporation residues were measured at projectile energies $\approx$4–7 MeV/A. At these energies, the identified residues are expected to be populated via CF and/or ICF of the projectile with the target nucleus. To understand the exact process involved in the ^{16}O + ^{51}V system, the experimentally measured EFs were analyzed within the frame of statistical model code ALICE-91 [30–32]. This code, developed by M. Blann, is used for the equilibrium as well as preequilibrium (PE) emission in light- and heavy-ion-induced reactions. In this code the compound nucleus (CN) calculations are performed by using Weisskopf-Ewing model [37] while preequilibrium emission is simulated by using a hybrid, geometry-dependent model [30,31]. The code ALICE-91 does not take ICF into account, and it can compute the statistical fission cross section utilizing Bohr-Wheeler approach [38] with angular-momentum-dependent ground state and saddle point energies. Detailed information about various parameters—like level density parameter (a), initial exciton number (n_o), mean free path (MFP) multiplier COST, etc.—used in this code for the calculations is mentioned in earlier work of our group [39,40] and also in Ref. [41]. The mean free path (MFP) is required to calculate intranuclear transition rates. As the calculated MFP for two body residual interactions may differ from the actual MFP, an adjustable parameter called mean free path multiplier COST is provided in this code to match the experimental and theoretical excitation functions. The level density parameter (a) largely affects the equilibrium emission, while the other parameters, initial exciton number (n_o), MFP multiplier and COST, govern the preequilibrium emission. The level density parameter is defined by the relation $a = A/K$, where A is the mass of the residual nuclei and K is an adjustable parameter which takes values to match the experimental data. The experimentally measured EFs were compared with ALICE-91 predictions for different values of level density parameters by using different K values (K = 8, 10, 12). As a representative case, the effect of variation of the parameter K on calculated EFs is presented in Fig. 2(a). In the present work, a value of $K = 8$ in general satisfactorily reproduces the experimental data for all complete fusion channels. Furthermore, the theoretical values of EFs with an optimized set of parameters were observed to be shifted towards the lower energy region compared to experimentally measured values [Fig. 2(a)]. This shift is expected and may be due to the large angular momentum of the projectile imparted to the composite nuclear system in case of HI-induced reactions. In ALICE-91, the compound nucleus (CN) calculations are performed by using the Weisskopf-Ewing model [37], which does not take into account the angular momentum effect. Hence, it is obvious to shift the theoretical EFs by an amount of nuclear rotational energy ($E_{\rm rot}$). A similar energy shift for theoretical EFs with ALICE-91 was also observed in some earlier work [23,24,40,41]. The estimated energy shift in excitation functions due to the angular momentum effect was calculated by using the expression for nuclear rotational

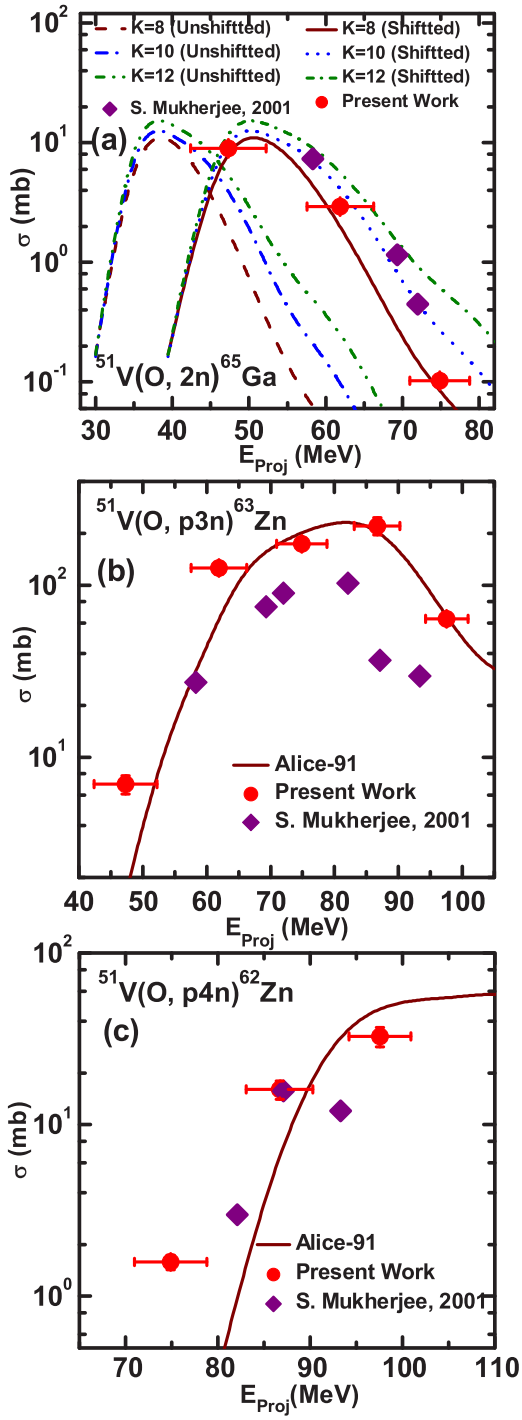

FIG. 2. Experimentally measured EFs (represented by red circles) of evaporation residues ^{65}Ga($2n$), ^{63}Zn($p3n$), and ^{62}Zn($p4n$) [panels (a)–(c)] are compared with ALICE-91 predictions. The present results for each evaporation residue are also compared with the work of Mukherjee [25]. The solid color lines represent the ALICE-91 predications with an energy shift equal to $E_{\rm rot}$ performed for $a = A/8$ MeV^{-1}.

energy $E_{\rm rot} = (m_P/m_T)E_{\rm lab}$, where m_P is the mass of the projectile, m_T is the mass of the target, and $E_{\rm lab}$ is the incident projectile energy. For evaporation residue ^{65}Ga($2n$), the experimentally measured EFs with an energy shift in theoretical EFs are shown in Fig. 2(a); note the agreement with the theoretical predictions. In the present work all the theoretical excitation functions for all evaporation residues have been shifted by $E_{\rm rot}$ on the energy scale, as shown in Figs. 2 and 3 by solid lines. However, we point out that the code ALICE-91 does not take ICF into account. Hence, the enhancement in the experimental cross section over the theoretical predications gives a clear indication of the incomplete fusion process.

A. *xn* and *pxn* channels

The measured EFs for ^{65}Ga($2n$), ^{63}Zn($p3n$), and ^{62}Zn($p4n$) evaporation residues are shown in Figs. 2(a)–2(c) and are expected to be populated via the complete fusion process. The available results for the same system of other workers [25] are also shown in the figure. It can be seen from Figs. 2(a) and 2(c) that, for $2n$ and $p4n$ channels, the present measurements and earlier reported values [25] are consistent with the theoretical predictions except for ^{62}Zn($p4n$) at energy 74.89 MeV. This discrepancy between the experimentally measured and theoretical values may be due to the contribution from its precursor ^{62}Ga($5n$). But for the $p3n$ channel, the results of Mukherjee *et al.* [25] are lower than present measurements and also than the theoretical predictions. Since, the ALICE-91 calculations are based on compound nucleus theory and do not take ICF into account, it is evident that the evaporation residues ^{65}Ga($2n$), ^{63}Zn($p3n$), and ^{62}Zn($p4n$) are formed by de-excitation of compound nucleus ^{67}Ga* via xn and/or pxn channels. The experimentally measured reaction cross-section for xn/pxn channels are shown in Table II.

B. αxn and $2\alpha xn$ channels

The experimentally measured EFs for α-emitting channels are shown in Fig. 3. Since these residues involve the emission of α particles, CF and/or ICF processes may be responsible for their production. The experimentally measured EFs of individual α-emitting channels are compared with ALICE-91 predictions calculated by using the same set of parameters as in the case of xn/pxn channels. From Fig. 3, it can be seen that for most of the α-emitting residues an enhancement has been observed in experimentally measured cross sections over the theoretically predicted cross sections. It can also be seen that the measured cross sections for the ^{61}Cu($\alpha 2n$) channel in the energy range ≈75 to 100 MeV are much higher then the theoretically obtained value and also do not follow the shape; however, at projectile energy ≈60 to 75 MeV, the measured EFs agree with theory. The measured cross sections for ^{60}Cu($\alpha 3n$) are in good agreement with the theoretical prediction up to projectile energy 90 MeV, and above that the measured value are higher than the theoretically calculated values. Further, the results of Mukherjee *et al.* [25] for ^{60}Cu($\alpha 3n$), underestimate present measurements as well as theoretical values. This may be due to the use of an incorrect γ-ray intensity taken by Mukherjee *et al.* Moreover, the measured cross-section values for ^{61}Co($\alpha 2p$), ^{58}Co($2\alpha n$), ^{57}Co($2\alpha 2n$), and ^{56}Co($2\alpha 3n$) residues are in good agreement

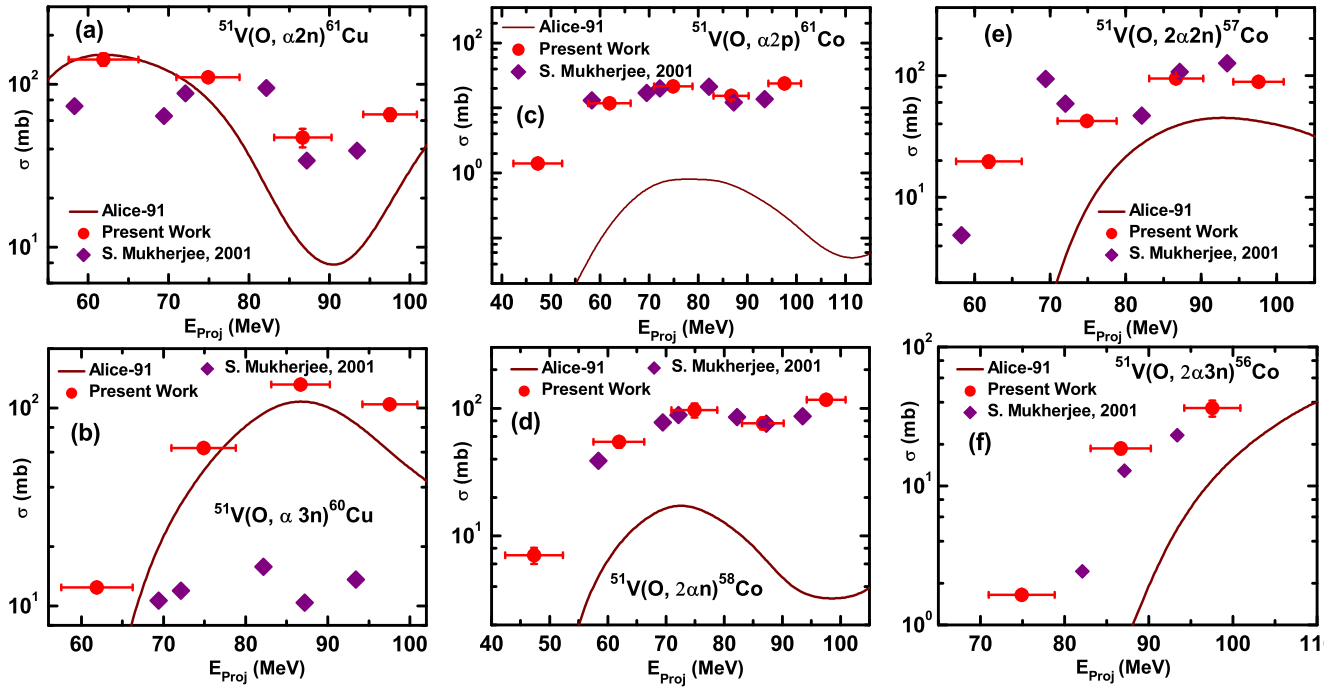

FIG. 3. Experimentally measured EFs (represented by red circles) of evaporation residues ^{61}Cu($\alpha 2n$), ^{60}Cu($\alpha 3n$), ^{61}Co($\alpha 2p$), ^{58}Co($2\alpha n$), ^{57}Co($2\alpha 2n$), and ^{56}Co($2\alpha 3n$) are compared with ALICE-91 predictions. The present results for each evaporation residue are also compared with the work of Mukherjee [25]. The solid color lines represent the ALICE-91 predictions with an energy shift equal to $E_{\rm rot}$ performed for $a = A/8$ MeV^{-1}.

with available literature values [25]. As mentioned in the previous section, the code ALICE-91 does not take ICF into account so any enhancement in the experimentally measured EFs over the theoretical predictions gives a clear indication of a contribution coming from incomplete fusion of the projectile. Thus for α-emitting channels, the evaporation residues may be populated via CF and/or ICF process. In such α-emitting channels, the following three decay processes may be involved: (i) the complete fusion of an^{16}O projectile with the target nucleus and formation of an excited compound nucleus ^{67}Ga* from which evaporation of neutrons and/or protons takes place; (ii) complete fusion of projectile ^{16}O with the target followed by the formation of an excited compound nucleus ^{67}Ga* from which evaporation of α particles and neutron and/or proton takes place; (iii) first the projectile ^{16}O breaks up into an α cluster (^{12}C + α and/or ^{8}Be + ^{8}Be and/or ^{8}Be + 2α) in the nuclear field of target nucleus (^{51}V), and then one of the fragments (^{12}C and/or ^{8}Be) fuses with the target nucleus forming an excited composite system from which the evaporation of neutron and/or proton takes place, while the remaining fragment (α and/or ^{8}Be and/or 2α) of the projectile goes on moving elastically in the forward cone as a spectator. Thus the α-emitting channels are expected to be populated via both CF and/or ICF processes. The enhancement observed in the experimentally measured cross section for exit channels over the ALICE-91 predictions may be attributed to the ICF

TABLE II. Experimentally measured production reaction cross sections σ (mb) of identified evaporation residues in the present system along with $\Sigma\sigma_{\rm CF}$, $\Sigma\sigma_{\rm ICF}$, $\Sigma\sigma_{\rm TF}$, and $F_{\rm ICF}(\%)$.

$E_{\rm lab}$	^{65}Ga (mb)	^{63}Zn (mb)	^{62}Zn (mb)	^{61}Cu (mb)	^{60}Cu (mb)	^{61}Co (mb)	^{58}Co (mb)
97.55 ± 3.33		63.79 ± 4.88	32.61 ± 4.31	65.17 ± 5.64	104.66 ± 1.96	23.66 ± 1.96	116.24 ± 8.73
86.68 ± 3.59		220.9 ± 24.72	16.04 ± 1.95	47.13 ± 6.05	131.57 ± 1.16	15.32 ± 1.82	76.41 ± 8.04
74.89 ± 3.92	0.102 ± 0.01	174.12 ± 13.23	1.585 ± 0.154	110.63 ± 2.63	62.86 ± 1.15	21.54 ± 2.35	96.52 ± 12.07
61.90 ± 4.35	2.92 ± 0.11	125.71 ± 10.4		142.47 ± 12.36	12.44 ± 0.649	11.88 ± 1.36	54.4 ± 5.37
47.29 ± 4.95	8.94 ± 0.8	6.96 ± 0.85				1.41 ± 0.12	7.03 ± 1.02

$E_{\rm lab}$	^{57}Co (mb)	^{56}Co (mb)	$\Sigma\sigma_{\rm CF}$	$\Sigma\sigma_{\rm ICF}$	$\Sigma\sigma_{\rm TF}$	$F_{\rm ICF}(\%)$
97.55 ± 3.33	88.64 ± 5.33	36.34 ± 4.9	1168.32	212.03	1380.34	15.36
86.68 ± 3.59	94.36 ± 3.71	18.6 ± 1.7	1146.96	148.51	1295.47	11.46
74.89 ± 3.92	42.22 ± 0.75	1.65 ± 0.13	1015.50	107.91	1123.41	9.61
61.90 ± 4.35	19.74 ± 2.17		789.79	46.43	836.22	5.55
47.29 ± 4.95			126.30	1.60	127.90	1.25

of the projectile. The contribution of ICF to the total fusion cross section depends upon the evaporation residue or the exit channel. The reaction mechanism involved in the formation of α and 2α emitting channels may be represented by different decay modes. For example, in the case of ^{60}Cu($\alpha 3n$) and ^{58}Co($2\alpha n$) channels, it can be inferred that the experimentally measured cross section for these two residue comes from the CF and/or ICF of the projectile through three different possible decay modes.

For α-emission case

(a) First way of CF of ^{16}O with ^{51}V: In this case, the CF of ^{16}O with ^{51}V forms an excited composite system which may decay via the $2p5n$ channel as

$$^{16}\mathrm{O} + {}^{51}\mathrm{V} \Rightarrow {}^{67}\mathrm{Ga}^{*} \Rightarrow {}^{60}\mathrm{Cu} + 2p5n;$$

i.e., the excited composite system decays via emission of $2p5n$.

(b) Second way of CF of ^{16}O with ^{51}V: In this case, the excited composite system may decay through the $\alpha 3n$ channel as

$$^{16}\mathrm{O} + {}^{51}\mathrm{V} \Rightarrow {}^{67}\mathrm{Ga}^{*} \Rightarrow {}^{60}\mathrm{Cu} + \alpha 3n;$$

i.e., the excited composite system may decay via the $\alpha 3n$ channel.

(c) Incomplete fusion of the projectile: This is another possible way in which the projectile incompletely fuses with the target nucleus; i.e., before fusion with the target nucleus, the projectile breaks up into its fragments (^{12}C and ^{4}He), one fragment (^{12}C) fuses with the target nucleus forming an incompletely fused composite system (^{63}Cu*) which may decay via emission of three neutrons ($3n$), and the remaining part of the projectile, i.e., an α cluster, goes on in the forward direction as a spectator, as

$$^{16}\mathrm{O}\,(^{12}\mathrm{C} + {}^{4}\mathrm{He}\ \text{or}\ \alpha) \Rightarrow {}^{12}\mathrm{C} + {}^{51}\mathrm{V} \Rightarrow {}^{63}\mathrm{Cu}^{*} \Rightarrow {}^{60}\mathrm{Cu} + \alpha\ (\text{as spectator}) + 3n.$$

For 2α-emission case

(a) First way of CF of ^{16}O with ^{51}V:

$$^{16}\mathrm{O} + {}^{51}\mathrm{V} \Rightarrow {}^{67}\mathrm{Ga}^{*} \Rightarrow {}^{58}\mathrm{Co} + 4p5n;$$

i.e., ^{67}Ga* decays via the $4p5n$ channel.

(b) Second way of CF of ^{16}O with ^{51}V:

$$^{16}\mathrm{O} + {}^{51}\mathrm{V} \Rightarrow {}^{67}\mathrm{Ga}^{*} \Rightarrow {}^{58}\mathrm{Co} + 2\alpha n;$$

i.e., here ^{67}Ga* decays via the $2\alpha n$ channel.

(c) ICF of ^{16}O with ^{51}V:

$$^{16}\mathrm{O}\,(^{8}\mathrm{Be} + {}^{8}\mathrm{Be}\ \text{or}\ 2\alpha) + {}^{51}\mathrm{V} \Rightarrow {}^{59}\mathrm{Co}^{*} + {}^{8}\mathrm{Be} \Rightarrow {}^{58}\mathrm{Co} + 2\alpha(\text{as spectator}) + n;$$

i.e., the incompletely fused system (^{59}Co*) may decay via the emission of a neutron.

Hence, from Fig. 3(b), it can be inferred that the residue ^{60}Cu($\alpha 3n$) may produce via ICF along with the CF process.

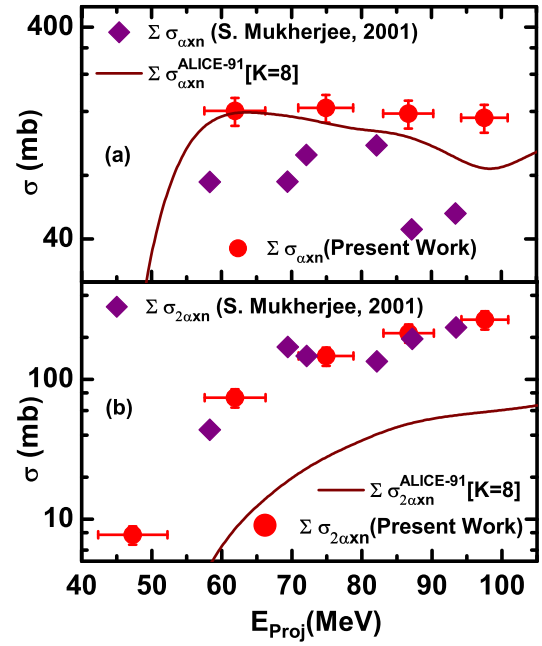

FIG. 4. (a) Sum of experimental cross sections for αxn channels. (b) Sum of experimental cross sections for $2\alpha xn$ channels. All these results are also compared with ALICE-91 predictions and earlier work (Mukherjee [25]).

At low energy there is agreement between experimental and theoretical values, while at energies above ≈74 MeV the experimental cross section starts increasing and shows an enhancement at increasing energy over the theoretical predictions, which indicates the contribution of ICF in ^{60}Cu($\alpha 3n$). However, theoretical predictions overestimate the experimentally measured cross section for this channel from the earlier work [25]. From the above observations, it can be concluded that ICF significantly contributes to the production of ^{61}Cu($\alpha 2n$) and ^{60}Cu($\alpha 3n$) for energies greater than 74 and 90 MeV respectively. Furthermore, for residues ^{61}Co($\alpha 2p$), ^{58}Co($2\alpha n$), ^{57}Co($2\alpha 2n$), and ^{56}Co($2\alpha 3n$), ICF is found to be of significant importance in the considered energy range. The experimentally measured cross-section values for these residues are depicted in Table II. For better understanding of ICF, the sum of experimental cross sections for $\alpha-$ and 2α-emitting channels i.e., $\Sigma\sigma_{\alpha xn}^{\text{expt.}}$ and $\Sigma\sigma_{2\alpha xn}^{\text{expt.}}$, have been plotted along with those calculated theoretically with ALICE-91 for the same set of input parameters and are shown in Fig. 4. From Fig. 4(a), it can be observed that initially at low energy the observed values of $\Sigma\sigma_{\alpha xn}^{\text{expt.}}$ show agreement with the theoretical predictions, and beyond 74 MeV, as the energy increases, a significant enhancement is observed over the theoretical predictions. Further, from Fig. 4(b), it can be seen that the reported values of $\Sigma\sigma_{2\alpha xn}^{\text{expt.}}$ are significantly higher than ALICE-91 predictions. Moreover, from Fig. 4(a), it can be observed that the $\Sigma\sigma_{\alpha xn}^{\text{ALICE-91}}$ values overestimate the $\Sigma\sigma_{\alpha xn}^{\text{expt.}}$ values obtained from the earlier work [25]. The observed enhancement in the measured EFs over theoretical values establish that ICF along with CF plays an important role in the production of these residues.

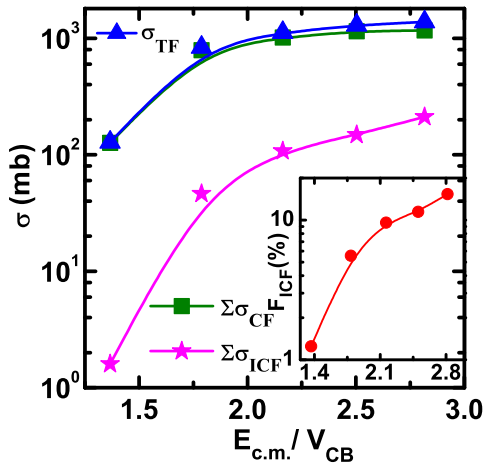

FIG. 5. The total fusion cross section (σ_{TF}) along with the sum of complete fusion and incomplete fusion cross sections ($\Sigma\sigma_{CF}$ and $\Sigma\sigma_{ICF}$), and in the inset the probability of incomplete fusion, are plotted as functions of reduced incident projectile energy (E_{cm}/V_{CB}).

IV. EFFECT OF ENTRANCE CHANNEL PARAMETERS ON ICF

The contribution of ICF in the production of α-emitting channels has been deduced as $\Sigma\sigma_{ICF} = \Sigma\sigma_{expt.} - \Sigma\sigma_{ALICE}$. Moreover, to see how much incompletely fused channels contribute to the total fusion cross section (σ_{TF}), the sum of cross sections of all CF channels ($\Sigma\sigma_{CF}$) along with σ_{TF} ($= \Sigma\sigma_{CF} + \Sigma\sigma_{ICF}$) as a function of reduced incident projectile energy (E_{cm}/V_{CB}) is plotted in Fig. 5. This figure shows that the separation between $\Sigma\sigma_{CF}$ and σ_{TF} increases with the projectile energy, which indicates energy dependence of ICF. Hence, in the inset of the Fig. 5, it is quite obvious that incomplete fusion probability of the projectile increases with the projectile energy. In order to study the dependence of incomplete fusion probability on different entrance channel parameters, the percentage of ICF fraction ($\%F_{ICF}$) or probability of ICF [$F_{ICF}(\%)$] has been deduced for the present system $^{16}O + ^{51}V$. The $F_{ICF}(\%)$ is a measurement of strength of ICF relative to total fusion, and is defined as $F_{ICF}(\%) = (\Sigma\sigma_{ICF}/\sigma_{TF}) \times 100$. The calculated percentages of ICF fraction are listed in Table II. To check the consistency of the present system with the previous work of Mukherjee *et al.* [25], evaluated percentage of ICF fraction is plotted in Fig. 6(a) along with the deduced ICF fractions for $^{20}Ne + ^{51}V$ [26] and $^{12}C + ^{51}V$ [27] systems. From this figure, it is clear that the $F_{ICF}(\%)$ is ≈2.0 to 3.5 times larger for the $^{20}Ne + ^{51}V$ system as compared to $F_{ICF}(\%)$ for the $^{12}C + ^{51}V$ system, and similarly, for the present system, $F_{ICF}(\%)$ is ≈1.6 to 2.7 times larger than the $F_{ICF}(\%)$ for the $^{12}C + ^{51}V$ system. This indicates that the ICF contribution for ^{20}Ne and ^{16}O projectiles is larger than the ICF contribution for the ^{12}C projectile. Hence, the present results show that the incomplete fusion probability may also depend upon the type of projectile. Moreover, this figure also shows a disagreement with the mass-asymmetry systematic, given by Morgenstern *et al.* [28].

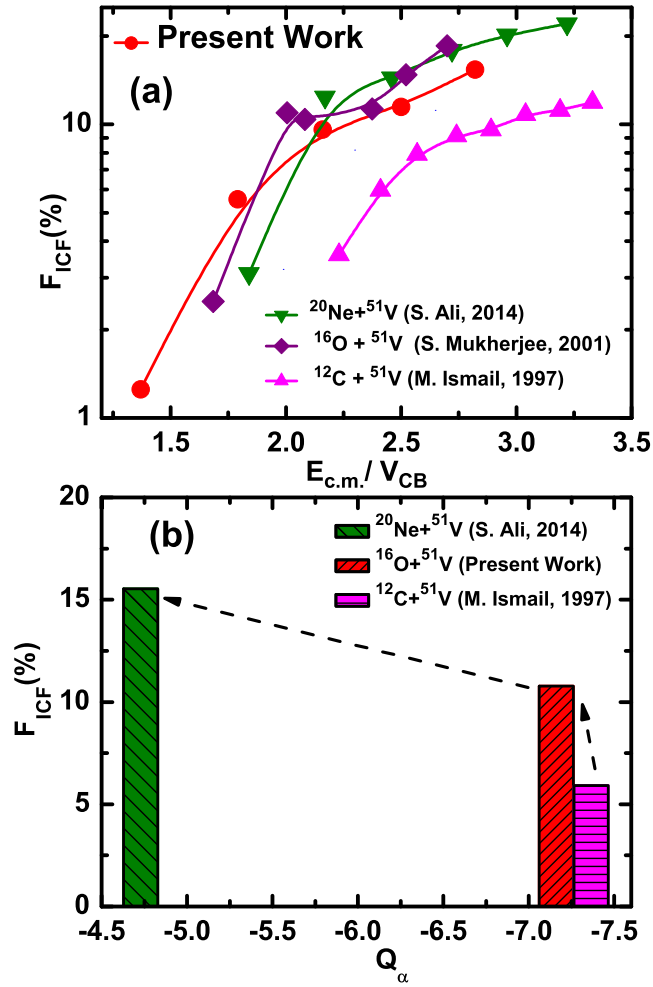

FIG. 6. (a) The probability of ICF [$F_{ICF}(\%)$] for the present system as a function of reduced incident projectile energy is compared with earlier work (Mukherjee [25], Ali [26], and Ismail [27]). (b) Comparison of $F_{ICF}(\%)$ as a function of α-decay Q value (Q_α) of projectile at constant relative velocity $V_{rel} = 0.081c$. The observed α-decay Q values for three projectiles, namely ^{20}Ne, ^{16}O, and ^{12}C, are −4.73, −7.16, and −7.37 MeV respectively.

According to mass-asymmetry systematics of Morgenstern *et al.*, the ICF reaction dynamics is governed by the relative velocity of the projectile and the mass asymmetry (μ_A) of the interacting partners. For different systems having different Coulomb barriers, the following expression has been used for the estimation of relative velocity of the projectile: $V_{rel} = [2(E_{cm} - V_{CB})/\mu]^{1/2}$, where μ is the reduced mass of the system, E_{cm} is the energy of the projectile, and V_{CB} is the fusion barrier in the center-of-mass frame. The mass asymmetry of the interacting partners is defined as $\mu_A = A_T/(A_T + A_P)$; where A_T is the mass of the target and A_P is the mass of the projectile. According to Morgenstern mass-asymmetry systematics, the ICF fraction for $^{12}C + ^{51}V$ system, being most mass asymmetric, must be greater than those for $^{16}O + ^{51}V$ and $^{20}Ne + ^{51}V$ systems. But, Fig. 6(a) reflects that the ICF fraction is least for the $^{12}C + ^{51}V$ system among the three. This disagreement can be explained in terms of various

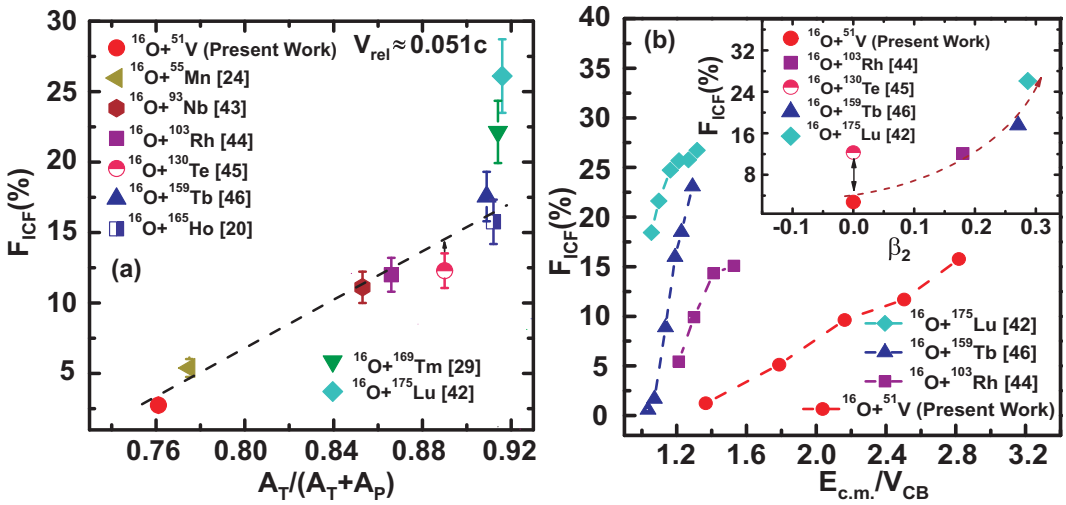

FIG. 7. (a) The deduced $F_{ICF}(\%)$ value for the present system along with those of previously studied systems (Kamal [20], Sunil [24], Singh [29], Harish [42], Anil [43], Unnati [44], Devendra [45], Manoj [46]), as a function of mass-asymmetry (μ_A), are plotted at $V_{rel} = 0.051c$. (b) The probabilities of ICF [$F_{ICF}(\%)$] for the present system and for three other systems [42,44,46], deduced from the available data for those systems, are shown as a function of reduced incident projectile energy. In the inset of Fig. 7(b), the deduced $F_{ICF}(\%)$ values for five systems are shown as a function of deformation parameter (β_2). The dashed lines are drawn in the figures just to guide the eyes.

physical parameters as in previous studies [20–24], where we have observed a projectile-structure-dependent mass- asymmetry. This projectile structure can be observable in terms of α-decay Q values of the projectile. To study the effect of α-decay Q value of the projectile, the observed α-decay Q values for three projectiles, namely ^{20}Ne, ^{16}O, and ^{12}C, are plotted with $F_{ICF}(\%)$ in Fig. 6(b). From the data presented in Fig. 6(b), it can be seen that the value of $F_{ICF}(\%)$ is found to be less for larger negative α-decay Q value of the projectile and shows a nonlinear dependence of $F_{ICF}(\%)$ on α-decay Q value of the projectile. The result is found to be consistent with the previous studies [20–24] and it can be concluded that the α-decay Q value is also important for the study of ICF reaction dynamics. Hence, the present observations suggest the inclusion of the projectile structure effect along with mass-asymmetry systematics [20–22] to explain ICF dynamics.

Moreover, if the projectile is the same with different targets systems, then projectile structure effect is normalized itself. So, in order to check the validity of the mass-asymmetry systematic for incomplete fusion processes, a systematic study was carried out for the present system ^{16}O + ^{51}V along with the available literature [20,24,29,42–46]. In Fig. 7(a), the value of $F_{ICF}(\%)$ for the present system ^{16}O + ^{51}V is plotted along with those obtained in Refs. [20,24,29,42–46] at a constant relative velocity (i.e., $V_{rel} = 0.051c$). As can be seen from this figure, incomplete fusion fraction increases gradually with the mass asymmetry of the interacting partners. In this figure, a steep increase in $F_{ICF}(\%)$ for ^{16}O + ^{169}Tm [29] and ^{16}O + ^{175}Lu [42] with increasing mass asymmetry is observed. Since we have plotted the mass-asymmetry systematic at a single relative velocity in this figure, to explore the rapid increase in the ICF fraction for the above-mentioned two systems [29,42] we have plotted the ICF fraction at different reduced incident projectile energies (E_{cm}/V_{CB}) in Fig. 7(b). From this figure, it can be seen that the ICF fraction increases rapidly for more mass-asymmetric systems with the increase in the projectile energy. Also, it was observed by Inamura *et al.* [47] that ICF processes are mainly due to peripheral interactions. Hence, this rapid change in ICF probability, in Fig. 7(a), can also be understood in terms of target deformation parameter (β_2). Detailed information about the nucleus deformation parameter (β_2) is given in Ref. [48]. The values of deformation parameter (β_2) for different target nuclei (^{51}V, ^{103}Rh, ^{130}Te, ^{159}Tb, and ^{175}Lu) mentioned in the inset of Fig. 7(b) are taken from *Atomic Data and Nuclear Data Tables,* Vol. 59 [49]. Now, in order to assess the effect of nucleus deformation on incomplete fusion (ICF), the probability of ICF [$F_{ICF}(\%)$] for the present system along with four other systems at a constant relative velocity ($V_{rel} = 0.051c$) was plotted as a function of deformation parameter (β_2) and is shown in the inset of Fig. 7(b). From the inset, it can be seen that $F_{ICF}(\%)$ increases with the increase in deformation parameter (β_2), as also discussed in the work of Singh *et al.* [50]. It may be noticed from the inset that $F_{ICF}(\%)$ for ^{16}O + ^{130}Te is larger than that of the present system, but the value of β_2 for these two systems is the same ($\beta_2 = 0$) for both (^{51}V and ^{130}Te). The larger value of $F_{ICF}(\%)$ for the ^{16}O + ^{130}Te system may be due to the larger value of mass asymmetry as compared to that of the present system. This can be seen from Fig. 7(a): the present system is less mass asymmetric as compared to the ^{16}O + ^{130}Te system [45]. So, it is expected that the system [45] has larger probability of ICF as compared to the present system. Hence, the present analysiss show that only one parameter is not able to explain ICF reaction dynamics. The present study also revealed that the nucleus deformation parameter (β_2) may also play an important role in ICF reaction dynamics along with the projectile dependent mass-asymmetry systematics.

V. SUMMARY AND CONCLUSION

To study the effect of various entrance channel parameters on fusion incompleteness, excitation functions for different ERs, namely ^{65}Ga($2n$), ^{63}Zn($p3n$), ^{62}Zn($p4n$), ^{61}Cu($\alpha 2n$), ^{60}Cu($\alpha 3n$), ^{61}Co($\alpha 2p$), ^{58}Co($2\alpha n$), ^{57}Co($2\alpha 2n$), and ^{56}Co($2\alpha 3n$), were measured in the $^{16}\mathrm{O} + {}^{51}\mathrm{V}$ interaction at energies of 4–7 MeV/A. The theoretical analysis for the present system was carried out in the framework of statistical model code ALICE-91. Results of previous work for the same system $^{16}\mathrm{O} + {}^{51}\mathrm{V}$ are also compared with the present analysis. There is no higher charge isobar precursor observed for any evaporation residue. The measured EFs for all xn/pxn channels are in agreement with the theoretical predictions of statistical model code ALICE-91, which reflects that the production of these residues is completely due CF processes. However, an enhancement has been observed for α-emitting channels for the same set of input parameters. This enhancement in the experimental cross section for α-emitting channels may be attributed to breakup of the projectile in the field of the target nucleus prior to fusion. In order to understand the ICF reactions for different parameters, the ICF fraction for the present system was also deduced. It is found that incomplete fusion probability of the projectile increases with the incident projectile energy. The present study shows that projectile structure is also responsible for fusion incompletenes,s which can be understood in terms of the α-decay Q value of the projectile. It is observed that the mass-asymmetry systematic is projectile structure dependent. Moreover, results of the present study show that ICF reactions are also affected by target deformation. In order to explore breakup processes in the vicinity of the Coulomb barrier, more systematic studies with different target-projectile combinations are required.

ACKNOWLEDGMENTS

The authors are thankful to the Director, IUAC, New Delhi, for providing all the necessary facilities to carry out the experiment. One of the authors, A.A., is thankful to Science and Engineering Research Board (SERB), Department of Science and Technology (DST), Government of India for financial support through research project EMR/2016/006983. The authors also extend their gratitude towards Dr. Sanjeev Saxena, Head, Department of Physics, Bareilly College, Bareilly (India) for his support and interest in this work. Thanks are also due to the operating crew of the Pelletron accelerator of IUAC for providing a stable beam.

[1] M. Dasgupta *et al.*, Phys. Rev. C **70**, 024606 (2004).
[2] F. Amorini *et al.*, Phys. Rev. C **58**, 987 (1998).
[3] F. K. Amanuel, B. Zelalem, A. K. Chaubey, A. Agarwal, I. A. Rizvi, A. Maheshwari, and T. Ahmed, Phys. Rev. C **84**, 024614 (2011).
[4] D. J. Hinde, M. Dasgupta, B. R. Fulton, C. R. Morton, R. J. Wooliscroft, A. C. Berriman, and K. Hagino, Phys. Rev. Lett. **89**, 272701 (2002).
[5] A. Agarwal *et al.*, Eur. Phys. J. Web Conf. **38**, 17001 (2012).
[6] A. Yadav *et al.*, Phys. Rev. C **85**, 064617 (2012).
[7] P. R. S. Gomes, R. Linares, J. Lubian, C. C. Lopes, E. N. Cardozo, B. H. F. Pereira, and I. Padron, Phys. Rev. C **84**, 014615 (2011).
[8] F. K. Amanuel *et al.*, Eur. Phys. J. A **47**, 156 (2011).
[9] P. R. S. Gomes *et al.*, Phys. Rev. C **73**, 064606 (2006); Phys. Lett. B **601**, 20 (2004).
[10] M. Dasgupta *et al.*, Nucl. Phys. A **787**, 144 (2007).
[11] P. P. Singh *et al.*, Phys. Rev. C **78**, 017602 (2008); **80**, 064603 (2009).
[12] H. C. Britt and A. R. Quinton, Phys. Rev. **124**, 877 (1961).
[13] J. Galin *et al.*, Phys. Rev. C **9**, 1126 (1974).
[14] R. Weiner *et al.*, Nucl. Phys. A **286**, 282 (1977).
[15] J. Wilczynski *et al.*, Nucl. Phys. A **373**, 109 (1982).
[16] T. Udagawa and T. Tamura, Phys. Rev. Lett. **45**, 1311 (1980).
[17] J. P. Bondorf, Nucl. Phys. A **333**, 285 (1980).
[18] M. Blann, Phys. Rev. C **31**, 295(R) (1985).
[19] D. J. Parker, J. J. Hogan, and J. Asher, Phys. Rev. C **39**, 2256 (1989).
[20] K. Kumar *et al.*, Phys. Rev. C **88**, 064613 (2013); **87**, 044608 (2013).
[21] D. P. Singh *et al.*, Phys. Rev. C **80**, 014601 (2009).
[22] A. Yadav *et al.*, Phys. Rev. C **86**, 014603 (2012).
[23] S. Dutt *et al.*, EPJ Web Conf. **66**, 03024 (2014).
[24] S. Dutt *et al.*, EPJ Web Conf. **86**, 00009 (2015).
[25] S. Mukherjee *et al.*, Eur. Phys. J. A **12**, 199 (2001).
[26] S. Ali *et al.*, J. Mod. Phys. **5**, 2063 (2014).
[27] M. Ismail *et al.*, Pramana J. Phys. **49**, 623 (1997).
[28] H. Morgenstern, W. Bohne, W. Galster, K. Grabisch, and A. Kyanowski, Phys. Rev. Lett. **52**, 1104 (1984).
[29] P. P. Singh, B. P. Singh, M. K. Sharma, Unnati, D. P. Singh, R. Prasad, R. Kumar, and K. S. Golda, Phys. Rev. C **77**, 014607 (2008).
[30] M. Blann, Phys Rev. Lett. **27**, 337 (1971).
[31] M. Blann, Phys Rev. Lett. **28**, 757 (1972).
[32] M. Blann, ALICE-91, report, LLNL/IAEA/NEA Data Bank, 1991 (unpublished).
[33] FREEDOM, data acquisition and analysis software, designed to support the accelerator based experiments at the Inter University Accelerator Center (IUAC), New Delhi, India.
[34] The Stopping and Range of Ions in Matter (SRIM) code, http://www.srim.org/SRIM/SRIMLEGL.htm
[35] B. P. Ajith Kumar *et al.*, CANDLE, Collection and Analysis of Nuclear Data using Linux nEtwork, in Proceedings of the DAE Symposium on Nuclear Physics, 2001, Kolkotta (unpublished).
[36] E. Browne and R. B. Firestone, *Table of Radioactive Isotopes* (Wiley, New York, 1986).
[37] V. F. Weisskopf and D. H. Ewing, Phys. Rev. **57**, 472 (1940).
[38] N. Bohr and A. Wheeler, Phys Rev. **56**, 426 (1939).
[39] A. Agarwal *et al.*, J. Phys. Soc. Jpn. **70**, 2903 (2001).
[40] A. Agarwal *et al.*, Int. J. Mod. Phys. E **17**, 393 (2008).
[41] M. K. Sharma *et al.*, Phys. Rev. C **70**, 044606 (2004); **91**, 014603 (2015).
[42] H. Kumar, Ph.D. thesis, A. M. University, Aligarh, India, 2017 (unpublished).
[43] A. Sharma *et al.*, J. Phys. G: Nucl. Part. Phys. **25**, 2289 (1999).

[44] U. Gupta *et al.*, Nucl. Phys. A **811**, 77 (2008).
[45] D. P. Singh, V. R. Sharma, A. Yadav, P. P. Singh, Unnati, M. K. Sharma, R. Kumar, B. P. Singh, and R. Prasad, Phys. Rev. C **89**, 024612 (2014).
[46] M. K. Sharma *et al.*, Nucl. Phys. A **776**, 83 (2006).
[47] T. Inamura *et al.*, Phys. Lett. B **68**, 51 (1977).
[48] S. Raman *et al.*, At. Data Nucl. Data Tables **78**, 1 (2001).
[49] P. Moller *et al.*, At. Data Nucl. Data Tables **59**, 185 (1995).
[50] D. Singh *et al.*, Phys. Rev. C **97**, 064610 (2018).